*Met. Mater. Int., Vol. 19, No. 4 (2013), pp. 667~671*
doi: 10.1007/s12540-013-4005-7

# Design of Ultrafine Eutectic-Dendrite Composites with Enhanced Mechanical Properties in Fe-Based Alloy

**T. E. Kim[1], S. W. Sohn[1], J. M. Park[1,2], C. W. Bang[1], W. T. Kim[3], and D. H. Kim[1,*]**

[1]Yonsei University, Center for Non-crystalline Materials, Department of Metallurgical Engineering, 134 Shinchondong Seodaemungu, Seoul 120-749, Korea
[2]Institute for Complex Materials, IFW Dresden, P.O. Box 27 01 16, D-01171 Dresden, Germany
[3]Cheongju University, IT Division, 36 Naedok Dong, Cheongju 360-764, Korea

(received date: 7 August 2012 / accepted date: 15 August 2012)

The effect of Mn content on the evolution of microstructure and the enhancement of mechanical properties in Fe-Nb-Mn hierarchical composites consisted of ultrafine eutectic and primary dendrite has been studied by using X-ray diffractometry, scanning electron microscopy, transmission electron microcopy and compression test. Fe-11Nb-5Mn hierarchical composite consisted of α′-Fe dendrite and urtrafine α′-Fe + $Fe_2Nb$ eutectic, and exhibited a reasonably good combination of mechanical properties, i.e. yield strength of 1283 ± 10 MPa and compressive plastic strain of 7.75 ± 5%, while Fe-11Nb-15Mn composite consisted of ε-Fe dendrite and ε-Fe + $Fe_2Nb$ eutectic structure with some retained γ phase, and exhibited a far better combination of mechanical properties, i.e. higher yield strength of 1462 ± 10 MPa and larger compressive plastic strain of 11.28 ± 2%. The origin for the simultaneous enhancement of high strength and large plastic strain is attributed to ε-Fe martensite formation and strain-induced martensitic transformation from ε to α′ during deformation.

**Key words:** composites, deformation, phase transformation, compression test, transmission electron microscopy, plasticity

## 1. INTRODUCTION

Many studies have been performed to develop a new advanced material having high strength and large ductility by using bimodal length scale distribution in the microstructure. Several composite materials consisted of nano-scale eutectic and micron-scale primary dendrite were produced by copper mold casting in eutectic alloy systems by adjusting alloy composition [1-9]. The nature of high strength in these composites comes from the complex fine network structure of the eutectic matrix. Furthermore, the plastic strain of the composites strongly correlated with the volume fraction and morphology of dendrite and length scale heterogeneity of microstructure [3,4]. Recently, transformation induced plasticity (TRIP)-aided metallic glass composites exhibiting enhanced plasticity have been developed [10-12]. For example, addition of Ti or Al in Cu-Zr based metallic glass composites induced martensitic transformation during deformation from B2-CuZr to B19′-CuZr similar to NiTi system showing shape memory behavior [10]. The TRIP aided metallic glass composites shows work hardening behavior, resulting in large compressive plastic strain, which is different from normal behavior of work softening in monolithic bulk metallic glasses.

It is well known that the TRIP aided steel offers a good combination of high strength and plastic strain, being compared with the conventional low alloy steel [13,14]. In TRIP aided steel, pre-existing retained austenite transformed to martensite during plastic deformation. Rapid casting process was often adopted to prepare an in-situ composites consisted of nano-scale eutectic and micron-scale dendrite phases in one step process [8]. The Fe solid solutions in eutectic and in dendrite structure experience various solid state transformation depending on the alloy chemistry and cooling rate during casting. In the case of Fe-based composites with $M_s$ temperature above the room temperature, the microstructural evolution includes a martensitis transformation from the austenite (γ) phase due to high cooling rate during casting [7]. In such a case, it is quite unlikely that TRIP effect will play a role in mechanical property enhancement. Therefore, it is important to control the stability of γ phase to suppress the extensive α′ martensitic transformation during cooling to optimize the TRIP effect for enhancement of mechanical properties.

For Fe-Mn system, it is well known that Mn is a γ stabilizing element and the high temperature γ-Fe phase can lead to martensitic transformations during cooling to ε-Fe and/or α′-

*Corresponding author: dohkim@yonsei.ac.kr

Fe [15-18]. The reaction products of Fe-Mn alloy vary depending on alloy composition [16]. In alloy with Mn content between 15 and 23 wt%, the γ→ε martensitic transformation can be induced by quenching from the high temperature. In alloys with more than 27 wt% Mn, the ε martensitic transformation is not detected. Moreover, in Fe-Mn alloy with low stacking fault energy, it is reported that strain-induced γ→ε→α′ and γ→α′ martensitic transformations easily occur during deformation.

In this study, we tried to control the stability of γ phase by controlling the austenite stabilizing element Mn with an aim to utilize TRIP effect for enhancement of mechanical properties. We report here the microstructure and mechanical properties of Fe-11Nb-xMn (x=5, 15) in-situ hierarchical composites, produced by suction casting.

## 2. EXPERIMENTAL PROCEDURES

Fe-11Nb-5Mn and Fe-11Nb-15Mn alloy ingots (wt%) were prepared by arc melting of high purity elemental constituents (99.9 wt%) under an argon atmosphere. The ingots were prepared by suction casting into copper mold having a cylindrical cavity with a diameter of 2 mm and a length of 50 mm. The cooling rate during solidification was estimated to be about ~$10^2$ K/s. Microstructural analysis of as-cast and deformed samples was performed by scanning electron microscopy (SEM, Hitachi, S-2700, Tokyo, Japan). X-ray diffractometry (XRD, Rigaku RINT2200, Cu Kα radiation, Tokyo, Japan) and transmission electron microscopy (TEM, JEM 2010F, Tokyo, Japan) coupled with energy-dispersive x-ray analysis (EDX, Oxford instrument INCA system, Oxfordshire, UK) were used for structural characterization and phase identification. Thin foil specimens for TEM observation were prepared by a conventional ion milling method (Precision Ion Polishing System, Gatan Model 691, Vienna, OH). In order to evaluate the mechanical properties in compression, cylindrical specimens with an aspect ratio of 2:1 were prepared and tested at room temperature under a quasi-static loading condition with an initial strain rate of $10^{-3}$ $s^{-1}$.

## 3. RESULTS AND DISCUSSION

Figures 1(a) and (b) show XRD patterns of as-cast Fe-11Nb-5Mn and Fe-11-15Mn rod specimens, respectively, together with analyzed results. The XRD pattern from Fe-11Nb-5Mn alloy shows the reflections corresponding to a mixture of body-centered cubic (bcc) α′-Fe (Im3m, a=0.286 nm) and a hexagonal closed packed ($P6_3/mmc$, a=0.4813 nm and C=0.7849 nm) $Fe_2Nb$ phases. The XRD pattern from Fe-11Nb-15Mn alloy shows diffraction peaks corresponding to a mixture of a face-centered cubic (fcc) γ-Fe (Fm3m, a=0.3597 nm), a hcp ε-Fe ($P6_3/mmc$, a=0.245 nm and c=0.393 nm) and a hcp $Fe_2Nb$ phases. The XRD analysis indicates

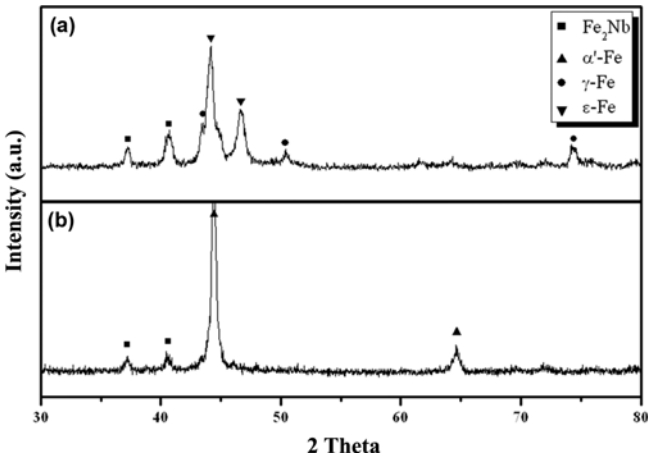


**Fig. 1.** XRD patterns of as-cast (a) Fe-11Nb-5Mn and (b) Fe-11Nb-15Mn rod samples.

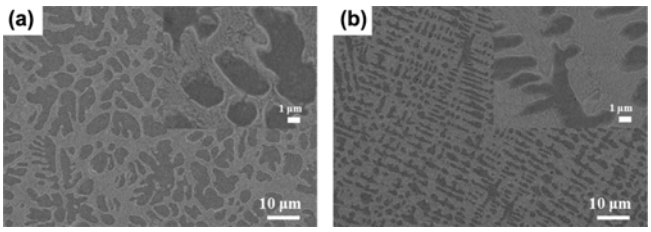


**Fig. 2.** SEM images obtained from (a) as-cast Fe-11Nb-5Mn and (b) Fe-11Nb-15Mn rod samples.

that the Fe-11Nb-15Mn alloy experiences partial martensitic transformation from austenite (γ-Fe) to ε martensite during cooling in solid state. The γ→ε martensitic transformation was commonly found in manganese steels during quenching from high temperature [16]. However, ε martensite was not found for Fe-11Nb-5Mn specimens, in which only α′ phase was found. These results indicate that the amount of Mn affects the phase transformation mode in Fe-Nb-Mn alloy system.

Figures 2(a) and (b) show back scattered images (BSE) of the as-cast Fe-11Nb-5Mn and Fe-11Nb-15Mn alloy specimens, respectively. Both microstructures were taken at the center of rod specimens. The as-cast Fe-11Nb-5Mn alloy shows typical hypoeutectic micostructure which consists of dark dendrite (α′-Fe) with a secondary dendrite arm spacing of about 10 μm and bright eutectic structure (α′-Fe+$Fe_2Nb$) with a lamellar spacing of 200-300 nm. Due to higher content of Nb in eutectic structure than in dendrite, eutectic region appears bright. The BSE micrograph of the Fe-11Nb-15Mn alloy shown in Fig. 2(b) exhibits again a hypo-eutectic structures in which dendrite are surrounded by ultrafine eutectic structure. Remember that the specimen consisted of retained γ-Fe, ε-Fe and $Fe_2Nb$, which was confirmed by X-ray diffractometry shown in Fig. 1(b) and TEM observation described in later. The dendrites of micron-scale are surrounded by a eutectic structure with ultrafine-scale which consists of ε-Fe and $Fe_2Nb$. The secondary dendrite arm spacing and volume faction of the den-

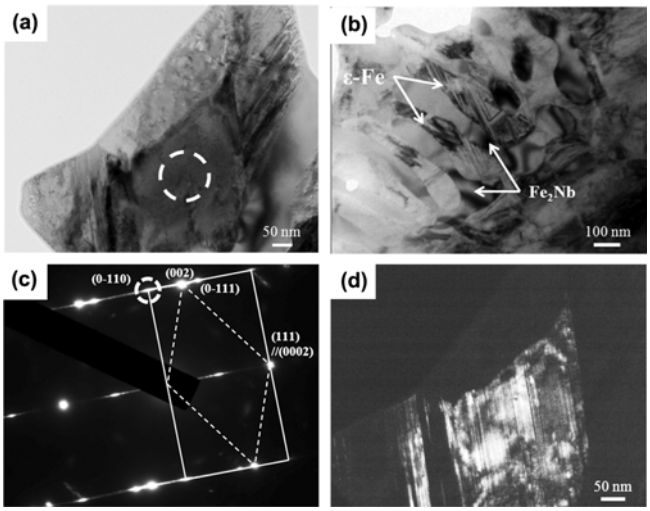


**Fig. 3.** TEM micrographs obtained from as-cast Fe-11Nb-15Mn alloy: (a) bright field image from dendritic region and (b) bright field image from eutectic region, (c) SADP from the dashed circle in Fig. 3(a) with analyzed result, and (d) dark-field TEM image taken using ε-Fe reflection from dashed circle in Fig. 3(a).

drites are 4-5 μm and around 50%, respectively. Moreover, the average eutectic lamellar spacing and the colony is 150-200 nm and 25-30 μm. The SEM image shows that the average lamellar spacing of eutectic matrix, the dendrite arm spacing of the primary dendrites and volume fraction of dendrites are about 150-200 nm, 4-6 μm and ~50%, respectively.

Figure 3 shows bright-field TEM images ((a) and (b)), selected area diffraction pattern (SADP) (c) and dark-field TEM image (d), obtained from the as-cast Fe-11Nb-15Mn alloy specimen. The TEM bright-field image in Fig. 3(a) shows an internal microstructure of the dendrite in Fe-11Nb-15Mn alloy. The dendritic phase consisted of several platelet packets with an internal structure, indicating the occurrence of solid state transformation during casting. Figure 3(c) shows an SADP taken from the dashed circle in Fig. 3(a) together with the indexing result. It can be analyzed into a superposition of diffraction patterns corresponding to the [2-1-10] zone axis of the hcp ε-Fe and [-110] zone axis of the fcc γ-Fe. Both ε-Fe and γ-Fe show an orientation relationship of $\{111\}_\gamma$, $<110>_\gamma // \{0001\}_\varepsilon$, $<-1010>_\varepsilon$, which is in agreement of previous results [15]. Figure 3(d) shows a dark-field image of the dashed circle area, taken using diffraction spot corresponding to $(01\text{-}11)_{\varepsilon\text{-Fe}}$ in Fig. 3(c), It shows that the apparent multiple platelets were comprised of thin ε martensitic plate and retained austenite. In the Fig. 3(c) bright portion corresponds to ε platelet and dark portion to retained austenite. Figure 3(b) shows a bright-field image taken from the eutectic region of Fe-11Nb-15Mn alloy. It shows a lamellar structure, consisted of $Fe_2Nb$ and ε-Fe phases, with an average lamellar spacing of 150-200 nm. The observation of ε-Fe in the eutectic structure indicates that partial martensitic transformation took place even in the ultrafine eutectic region. The martensitic transformation in the confined region results in refinement of platelet packet size, which can be found in Fig. 3(b).

Micro compositional analysis was performed to measure local composition of primary dendrite and eutectic. Much care was taken to minimize the effect of surroundings in measuring the local composition. EDS experiments show $Fe_{82.1}Nb_{2.3}Mn_{15.7}$ and $Fe_{82.4}Nb_{2.1}Mn_{15.5}$ compositions for dendrite and Fe region in eutectic structure, respectively. The empirical formula of Ms temperature estimation is as follows [19]:

$$Ms(°C, at.\%) = 545 - 71C - Al + 7Co - 14Cr - 15Cu - 23Mn - 8Mo - 6Nb - 13Ni - 4Si + 3Ti - 4V - 0W$$

Following this formula, $M_s$ temperatures of dendrite phase and eutectic region are 170.8 °C and 175.15 °C, respectively. Therefore, The $M_s$ temperature of dendrite phase and eutectic region has an almost same composition with about 170 °C. The γ→ε martensitic transformation in Fe-Mn systems is affected by the stacking fault energy of the γ phase because the formation of ε-Fe is strongly related to the generation and movement of partial dislocations. As the stacking fault energy becomes lower, the γ→ε martensitic transformation can occur more easily. Lee and Choi [18] reported that the stacking fault energy of the γ phase decreases with Mn content, reaches minimum at 13 at.% Mn and then increase with further increase in Mn content. It may suggest that Fe-11Nb-15Mn alloy has larger driving force for ε martensite formation than that of Fe-11Nb-5Mn alloy. It may explain the formations of ε-Fe in the former and α′-Fe in the latter, observed in this study.

The microstructure and phase analysis of Fe-11Nb-5Mn alloy revealed that the alloy consists of α′ martensite dendrite and eutectic structure consisted of alternating α′ martensite and $Fe_2Nb$ lamellae. This result is in line with previous report that phase transformation mode in Fe-Mn system varies with Mn contents [20]. In alloy with Mn content lower than 10 wt%, the γ→α′ martensitic transformation took place on cooling, inhibiting the formation of the ε phase. In alloy with Mn content of 15-20 wt%, the γ→ε martensitic transformation can be induced by quenching from high temperature.

Figure 4 shows room temperature engineering stress strain curves of the as-cast Fe-11Nb-5Mn and Fe-11Nb-15Mn alloys under a uniaxial compression mode. The room temperature engineering stress-strain curve reveals values of 0.2% offset yield stress ($\sigma_y$), ultimate compressive stress ($\sigma_{max}$), plastic strain ($\varepsilon_p$) for Fe-11Nb-5Mn alloy of 1240 ± 10 MPa, 1540 ± 10 MPa, 7.2 ± 3%, respectively. The Fe-11Nb-15Mn alloy shows yield stress (1460 ± 10 MPa), ultimate compressive stress (1950 ± 10 MPa) and plastic strain (11.3 ± 3%), indicating an improvement of both strength and plasticity by increasing Mn content. It reveals that mechanical properties are strongly

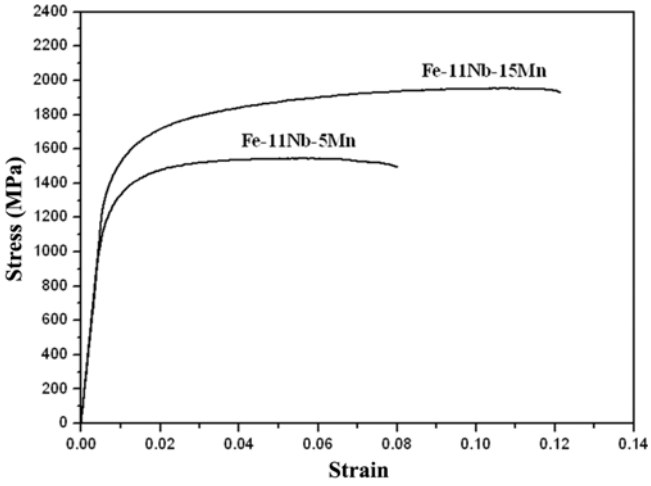


**Fig. 4.** Room temperature engineering stress-strain curves for the as-cast Fe-11Nb-5Mn and Fe-11Nb-15Mn rod samples.

dependent of the existing phase of Fe in dendrite and eutectic region. In case of Fe-Nb-Mn system, yield stress, ultimate stress and plastic strain dramatically increased with the presence of ε phase in dendrite and eutectic region.

In order to figure out the plastic deformation mode of Fe-11Nb-15Mn alloy with ε martensite dendrite embedded in the ultrafine eutectic matrix consisting of ε martensite and $Fe_2Nb$, the microstructure of sample after deformation has been investigated by HREM. During deformation strain induced martensitic transformation occurred. Figure 5(a) shows a HREM image, showing the co-existence of α′-Fe and ε-Fe phase in deformed Fe-11Nb-15Mn alloy specimen. Figures 5(b) and (c) show, respectively, Fourier transformed patterns from the α′-Fe and ε-Fe regions marked by dotted rectangle in the HREM image. The patterns in Figs. 5(b) and (b) correspond to [111] zone of α′-Fe and [2-1-10] zone of ε-Fe respectively. Figure 5(d) shows inverse Fourier transformed HREM image from the diffraction pattern of deformed sample. The HREM image in Fig. 5(a) clearly displays α′-Fe of about 20 nm size and α′/ε interface ahead of deformation direction by marked white arrow and α′-Fe. It is inferred that the nucleation of α′-Fe occurs from ε martensite during deformation. This suggests that ε→α′ strain induced martensitic transformation took place during compressive deformation. The orientation relationship between α′-Fe and ε-Fe was obtained to be $(110)_{\alpha'\text{-Fe}}//(0001)_{\varepsilon\text{-Fe}}$ and $[111]_{\alpha'\text{-Fe}}//[2\text{-}1\text{-}10]_{\varepsilon\text{-Fe}}$ from the Fourier transformed patterns shown in Fig. 5(b) and (c). This orientation relationship is in good agreement with previous report on the orientation relationship of γ/ε and α′/ε [15]:

$$\{111\}_{\gamma}, <110>_{\gamma}//\{0001\}_{\varepsilon}, <\text{-}1010>_{\varepsilon}//\{110\}_{\alpha'}, <111>_{\alpha'}.$$

To investigate atomic movement during ε→α′ martensitic transformation, Fourier transformed patterns (Fig. 5(b) and (c)) take inverse Fourier transformed image. Figure 5(d) shows

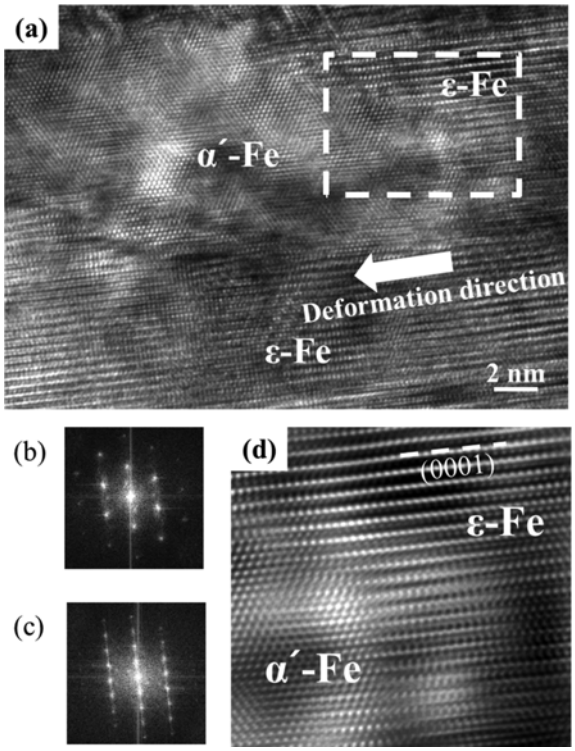


**Fig. 5.** (a) HRTEM image obtained after compression test in Fe-11Nb-15Mn alloy, (b) and(c) Fourier transformed patterns from α′-Fe and ε-Fe regions,respectively, in the dotted rectangle in the HREM image, and (d) the inverse Fourier transformed image of the ε/α′ interface.

Fourier transformed filtered image along the $[111]_{\alpha'\text{-Fe}}$ direction. The movement of (0001) planes of ε phase in ε/α′ interface and lattice distortion was observed in Fig. 5(d). These observations directly show plane movements of ε→α′ martensitic transformation. Atomic displacement in the strain induced ε→α′ martensitic transformation is investigated by Venables basically [21]. Also, Fujita reported a nucleation and growth mechanism in strain induced ε→α′ [22]. It is good agreement in Fourier transformed filtered image in Fig. 5(d).

These observation indicates that the enhanced mechanical properties of Fe-11Nb-15Mn alloy, being compared with those of Fe-11Nb-5Mn alloy, are attributed to the existence of ε-Fe phase in as-solidified specimen as shown in Figs.1 and 3, and to deformation induced ε→α′ transformation shown in Fig. 5. Especially, the existence of ε-Fe in ultrafine eutectic structure shown in Fig. 3(b) seems to play an important role in improving the plasticity, as shown in Fig. 4. The partial transformation from ε→α′ in the eutectic region can absorb strain energy during deformation and delay the formation of crack in the eutectic region. Finally the Fe-11Nb-10Mn hierarchical composites shows both significantly enhanced strength and compressive elongation, compared with those of Fe-11Nb-5Mn hierarchical composites consisted of α′-Fe dendrite and α′-Fe+$Fe_2Nb$ eutectic structure.

## 4. CONCLUSIONS

As-suction cast Fe-11Nb-5Mn alloy showed hierarchical composites consisted of α′-Fe dendrite and ultrafine α′+ $Fe_2Nb$ eutectic structure and yield strength (1283 ± 10 MPa) and compressive plastic strain (7.75 ± 5%). Fe-11Nb-15Mn alloy showed composite microstructure consisted of ε-Fe dendrite and ultrafine ε-Fe + $Fe_2Nb$ eutectic structure with some retained γ phase and yield strength (1462 ± 10 MPa) and compressive plastic strain (11.28 ± 2%). The origin of both high strength and large plastic strain in Fe-11Nb-15Mn alloy is attributed to ε-Fe martensite formation and strain-induced martensitic transformation from ε to α′ during deformation.

## ACKNOWLEDGMENTS

This work was supported by Defense Acquisition Program Administration (DAPA) and Agency for Defense Development (ADD), and also supported by the Global Research Laboratory Program of Korea Ministry of Science and Technology. T.E. Kim acknowledges the support from the Second Stage of Brain Korea 21 Project in 2011.

## REFERENCES

1. G. He, J. Eckert, W. Loser, and L. Schultz, *Nat. Mater.* **2**, 33 (2003).
2. D. V. Louzguine-Luzgin, L. V. Louzguina-Luzgina, H. Kato, and A. Inoue, *Acta. Mater.* **53**, 2009 (2005).
3. J. M. Park, S. W. Sohn, T. E. Kim, D. H. Kim, K. B. Kim, and W. T. Kim, *Scr. Mater.* **57**, 1153 (2007).
4. J. M. Park, K. B. Kim, W. T. Kim, M. H. Lee, J. Eckert, and D. H. Kim, *Intermetallics* **16**, 642 (2008).
5. T. E. Kim, J. M. Park, S. W. Sohn, D. H. Kim, W. T. Kim, M. Stoica, U. Kühn, and J. Eckert, *Mater. Trans.* **51**, 799 (2010).
6. J. M. Park, D. H. Kim, K. B. Kim, M. H. Lee, W. T. Kim, and J. Eckert, *J. Mater. Res.* **23**, 2003 (2011).
7. T. E. Kim, J. M. Park, U. Kühn, J. Eckert, W. T. Kim, and D. H. Kim, *Mater. Sci. Eng. A-Struct.* **531**, 51 (2012).
8. B. B. Sun, M. L. Sui, Y. M. Wang, G. He, J. Eckert, and E. Ma, *Acta. Mater.* **54**, 1349 (2006).
9. K. Song, J. Lee, J. Park, and K. Kim, *Met. Mater. Int.* **15**, 175 (2009).
10. S. Pauly, J. Das, J. Bednarcik, N. Mattern, K. B. Kim, D. H. Kim, and J. Eckert, *Scr. Mater.* **60**, 431 (2009).
11. D. C. Hofmann, *Science* **329**, 1294 (2010).
12. S. Pauly, S. Gorantla, G. Wang, U. Kühn, and J. Eckert, *Nat. Mater.* **9**, 473 (2010).
13. D. Fahr, *Metall. Mater. Trans. B-Proc.* **2**, 1883 (1971).
14. C. Y. Choi, I.-B. Kim, Y. Kim, and Y.-D. Park, *Korean J. Met. Mater.* **50**, 136 (2012).
15. R. L. Grunes, C. D'Antonio, and K. Mukherjee, *Mater. Sci. Eng. A-Struct.* **9**, 1 (1972).
16. J. Martínez, S. M. Cotes, A. F. Cabrera, J. Desimoni, and A. F. Guillermet, *Mater. Sci. Eng. A-Struct.* **408**, 26 (2005).
17. S. Cotes, M. Sade, and A. F. Guillermet, *Metall. Mater. Trans. A* **26**, 1957 (1995).
18. Y. K. Lee and C. S. Choi, *Metall. Mater. Trans. A-Phys.* **31**, 355 (2000).
19. K. Ishida, *J. Alloy. Compd.* **220**, 126 (1995).
20. H. Schumann, *Arch. Eisenhüttenwes* **38**, 10 (1967).
21. J. A. Venables, *Philos. Mag.* **7**, 35 (1962).
22. H. Fujita and T. Katayama, *Mater. Trans.* **33**, 243 (1992).